THE JOURNAL OF PHYSICAL CHEMISTRY B

pubs.acs.org/JPCB

Article

Morphology of Lyotropic Myelin Figures Stained with a Fluorescent Dye

Dominika Benkowska-Biernacka, Ivan I. Smalyukh, and Katarzyna Matczyszyn*

Cite This: *J. Phys. Chem. B* 2020, 124, 11974–11979

Read Online

ACCESS | Metrics & More | Article Recommendations | Supporting Information

ABSTRACT: Lyotropic myelin figures (MFs), i.e., long cylindrical structures formed by certain surfactants, owe their name to their resemblance to the biological membrane that covers nerve fibers. Herein, we used a strong bilayer-forming zwitterionic phospholipid stained by the Nile Red dye to study lamellar mesophases. Polarized optical microscopy and fluorescence confocal microscopy allowed us to investigate the morphology of myelin structures and determine the orientational order of amphiphilic molecules. The cross-sectional views reveal significant differences in the configurations of MFs within the liquid crystalline cell, as well as the details of a spontaneous and stimulated formation of branched lipid tubes. Our results provide insights into small-scale morphology and out-of-equilibrium structural changes in the multilamellar structures.

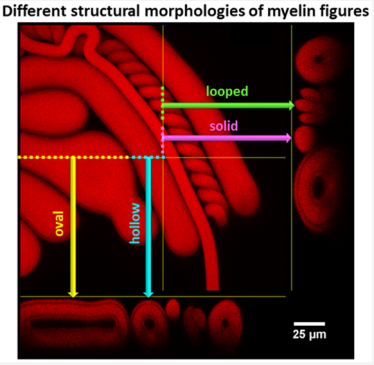

INTRODUCTION

There has been a growing interest in the studies of lyotropic liquid crystals (LLC) due to their essential role in diverse biological systems.[1−5] The well-known example of an LLC is myelin sheath, which is responsible for the efficient propagation of action potential between neurons. This structure is mainly composed of lipids that form stacked bilayers in an aqueous medium.[6] The natural myelin shows birefringence that is caused by the alignment of its amphiphilic molecules, among which phospholipids constitute about 40%.[7] Since myelin is related to the most prevalent autoimmune disease that affects the human brain and the spinal cord,[8] a possibility to mimic self-organization of this membrane is crucial for better understanding of lipid behavior in the lamellar phase and its biological significance.

Myelin was observed under polarized light microscope as elongated cylindrical tubules by Virchow for the first time as early as in 1854[9] and numerous investigations on artificial analogs of this structure were conducted since then, but there is still a lack of comprehensive and universally accepted knowledge about the formation of myelin structure. So far, there are several models to explain the origin of the growth mechanism of myelin tubes. For example, using tracking particles, Buchman confirmed that formation of a multibilayered tubule is caused by swelling rather than by diffusion process.[10] Tayebi et al. indicated that myelin growth occurs due to the presence of a driving force which is the humidity gradient.[11] According to Zou, the formation of myelin figures (MFs) might be also attributed to shear stress.[12] Moreover, microstructures consisting of multilamellar tubules are strongly influenced by many factors, including humidity, temperature,[11] pH,[13] and magnetic[14] and electric fields.[15] It was also shown that the morphology of MFs might be influenced by the contact between a surfactant and a substrate. Tubes formed from the pinned and the unpinned regions of the same sample exhibit differences in the core-to-wall thickness ratio, which is related to distinct membrane tensions.[16,17]

Typical MFs are formed by lyotropic lamellar mesophases, for instance, ones built of lipids[18,19] and ionic[20] or nonionic[21] surfactants in aqueous solution; however, MFs were also observed in systems with thermotropic smectic-A phase of liquid crystals.[22] Here, we used phospholipids, which can self-organize into bilayers owing to their cylindrical geometry[23] (Figure 1). While a significant amount of research has been conducted to study multilamellar lipid tubes by fluorescence microscopy,[16,24] surprisingly little attention has been paid to the examination of different structural morphologies of MF by confocal fluorescence microscopy, which offers a powerful tool to image cross-sectional views with diffraction-limited resolution also along the microscope's axis.

In the present article, we examine the liquid crystalline phase of MFs under a polarized light microscope equipped with a heating stage. According to the contact method, microstructures consisting of various forms of multilamellar tubules (e.g., looped and oval structures) were fabricated by hydration

Received: September 30, 2020
Revised: November 17, 2020
Published: December 21, 2020

https://dx.doi.org/10.1021/acs.jpcb.0c08907
J. Phys. Chem. B 2020, 124, 11974–11979

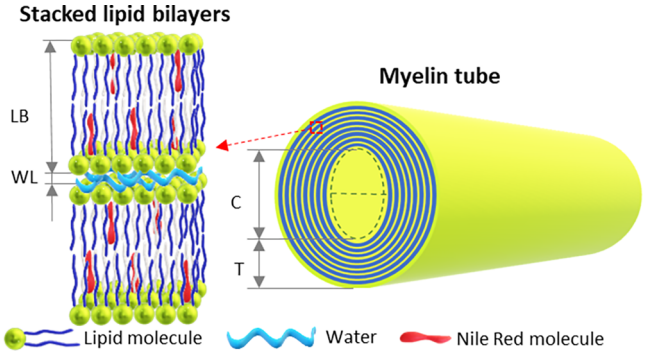

Figure 1. Schematic illustration of phospholipid bilayers (LB) separated by the water layer (WL) stained by Nile Red and (right) the multilamellar tube composed of stacked bilayers with the core of water (C). *T* denotes the thickness of the tube. (The dimensions are not to scale.).

of dried film made of phosphatidylcholines. Most importantly, we show the first reported observation of the spontaneous formation of side myelin structure in which the diameter and length are significantly smaller than in a primary myelin tube. The morphology of complicated forms of multilayered structures was studied by confocal fluorescence microscopy. The Nile Red dye, which spontaneously self-aligns along hydrocarbon chains of phospholipids, was used as a strongly fluorescent probe of orientational order in the presence of lipid-rich environment.[25,26]

EXPERIMENTAL SECTION

Materials. 1,2-Dilauroyl-*sn*-glycero-3-phosphocholine (DLPC) that was used for this study was purchased Avanti Polar Lipids. The phospholipid was dissolved in chloroform (purity >99%). 9-Diethylamino-5H-benzo[α]phenoxazine-5-one (Nile Red), which was applied as a fluorescence dye, was purchased from Biotium. All of these chemicals were used without further purification.

Sample Preparation. First, 0.3 mM solution of lipid coloring agent was prepared by dissolving Nile Red in chloroform. Then, the lipid solution was prepared by vigorous mixing of the defined amount of DLPC with Nile Red stock solution (final concentration, 60 mg/mL). A drop of lipid solution (1 μL) was placed on microscope glass and kept overnight to enable the evaporation of the solvent. Further, the plaque of lipids was sandwiched between a glass substrate and a coverslip fixed with a 30 μm spacing. After cell preparation, Milli-Q water was injected into the lipids by capillary flow at room temperature. Next, bilayers of amphiphilic molecules separated by a water layer started to self-organize into elongated structures starting from the dried lipid aggregates−water interface. Finally, the edges of the sample were protected by epoxy glue against fast solvent evaporation.

Myelin Figure Characterization. Polarized light microscopy was used to directly visualize myelin tubes. Images were taken by an Olympus BX60 optical microscope with and without a 530 nm retardation plate. The microscope was equipped with a temperature-controlled Linkam LTS120 stage. The morphology of myelin tubes was determined by confocal fluorescence microscopy. These studies were carried out using an Olympus FV3000RS confocal microscope equipped with a 60× oil immersion objective. A 561 nm laser was used as the fluorescence excitation source. The fluorescence emission was recorded in the spectral region from 580 to 655 nm. Scans along the *z*-axis were performed using a stepper motor by adjusting the focal plane position within the sample with a depth interval of 0.3 μm. Image analysis was performed using the Olympus Fluoview software. The orientation of phospholipids stained by anisotropic NR molecules in lamellar mesophase was investigated by fluorescence confocal polarizing microscopy.[27] The observations were performed using an Olympus IX81 inverted microscope equipped with a 100× oil immersion objective. The incident excitation laser beam (488 nm Ar laser) was linearly polarized, with its polarization controlled using a half-wave plate. The emitted signal was epi-collected with the same objective in the range from 560 to

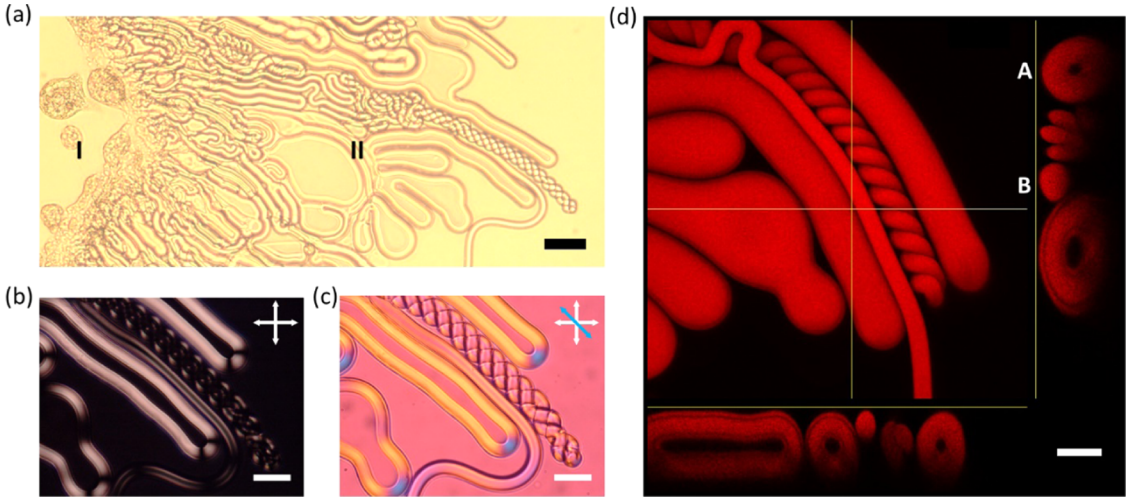

Figure 2. (a) Bright-field image of (II) multilamellar phase formation from (I) the lipid reservoir. The corresponding polarized light microscopy images of myelin figures were taken (b) without and (c) with a retardation plate. The arrows indicate the orientations of crossed polarizers (white double arrows) and the full-wavelength retardation plate's slow axis (blue double arrow). (d) Confocal fluorescent image of myelin figures stained by Nile Red. The vertical and horizontal lines indicate spatial locations at which the cross-sectional confocal views of myelin tubes were obtained (displayed on the right-hand side and below the plan view, respectively). Fluorescent images of "hollow" and "solid" cross-sectional views are marked with "A" and "B", respectively. The scale bars are (a) 50 μm and (b−d) 25 μm.

https://dx.doi.org/10.1021/acs.jpcb.0c08907
J. Phys. Chem. B 2020, 124, 11974−11979

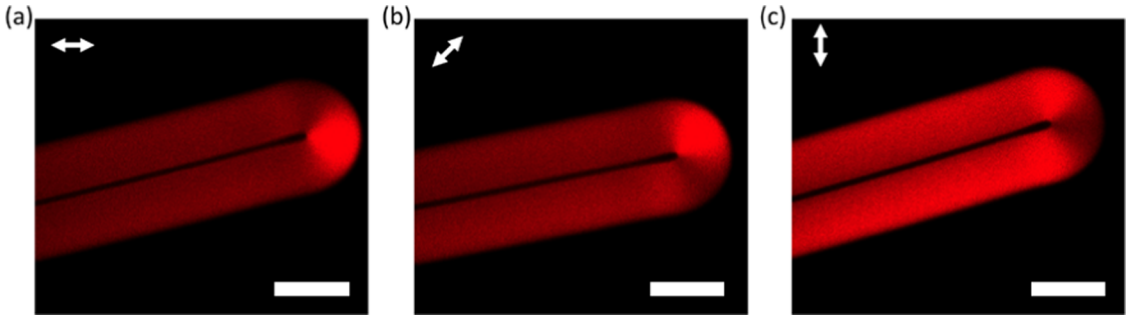

Figure 3. Fluorescent confocal polarizing images of the myelin tube labeled with Nile Red. The white double arrows indicate the polarization of the probing light used for the FCPM imaging. The scale bars are 10 μm.

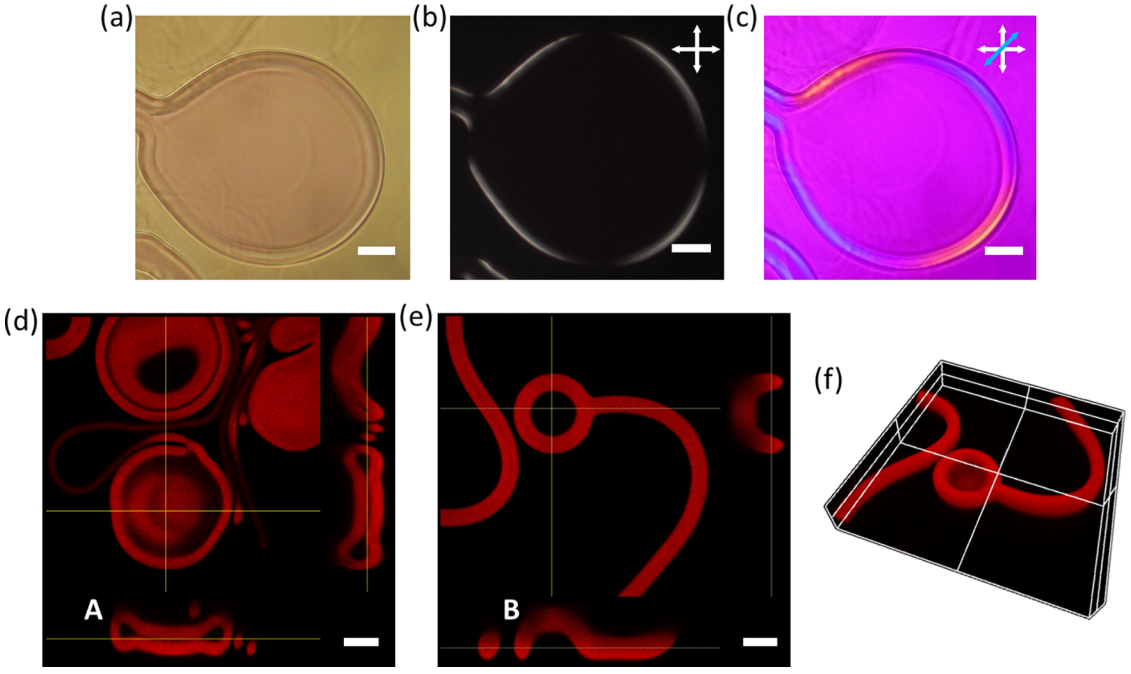

Figure 4. (a) Bright-field image and the corresponding polarizing light microscopy images of the myelin figure obtained (b) without and (c) with a retardation plate. The arrows indicate the orientations of crossed polarizers (white double arrows) and the full-wavelength retardation plate's slow axis (blue double arrow). (d,e) Fluorescent images of myelin figures ended with an oval shape with (A, B) cross-sectional views. (f) *Z*-projection of the myelin figure corresponding to (e). The white frame limits the field of view. The scale bars are 15 μm (a–c) and 25 μm (d, e).

600 nm selected by optical filters, with the linear polarization direction in the detection channel matching that of the excitation light.

RESULTS AND DISCUSSION

In all experiments, myelin structures were obtained from phospholipids doped with Nile Red using the contact experiment. As a consequence of the preparation method, spontaneous growth of MFs was directed toward the aqueous phase from the DPLC–water interface (Figure 2a). Considering the growth rate within the first minute of hydration, the growth process is divided into three regimes.[18]

It was shown that tubes with various diameters quickly increase in length, while maintaining a constant width of a few microns (Figures S1 and S2). After the first minute of rapid growth, further growth is substantially slower and enables formation of different types of multilayered microstructures.[28] Due to the strongly responsive behavior, the samples with lyotropic lamellar phases were sensitive to external factors, such as change of position and temperature. However, they can be clearly observed under a polarized light microscope from several hours to 2–3 days under constant conditions.

Different structural morphologies of multilamellar tubes can be observed under crossed polarizers (Figure 2b). To determine the orientation of lipids in bilayer membrane, an additional full-wave retardation plate (530 nm) was used.[29] Figure 2c depicts interference colors indicating alignment of amphiphilic molecules in multilamellar structure. The blue second-order interference color shows regions where lipids are oriented along the slow axis of the full retardation plate, whereas the yellow first-order interference color marks places where the lipid orientations within the lamellar phase are at 90° relative to the waveplate's slow axis.

To investigate the three-dimensional morphology of the obtained microstructures, confocal fluorescence microscopy was used. Figure 2d represents the fluorescent image of different types of lipid tubes formed 15 min after the sample cell preparation. Consistent with a previous report,[16] we observe MFs with and without an explicit core that are named hollow and solid tubes, respectively. The solid cross-sectional

https://dx.doi.org/10.1021/acs.jpcb.0c08907
J. Phys. Chem. B 2020, 124, 11974–11979

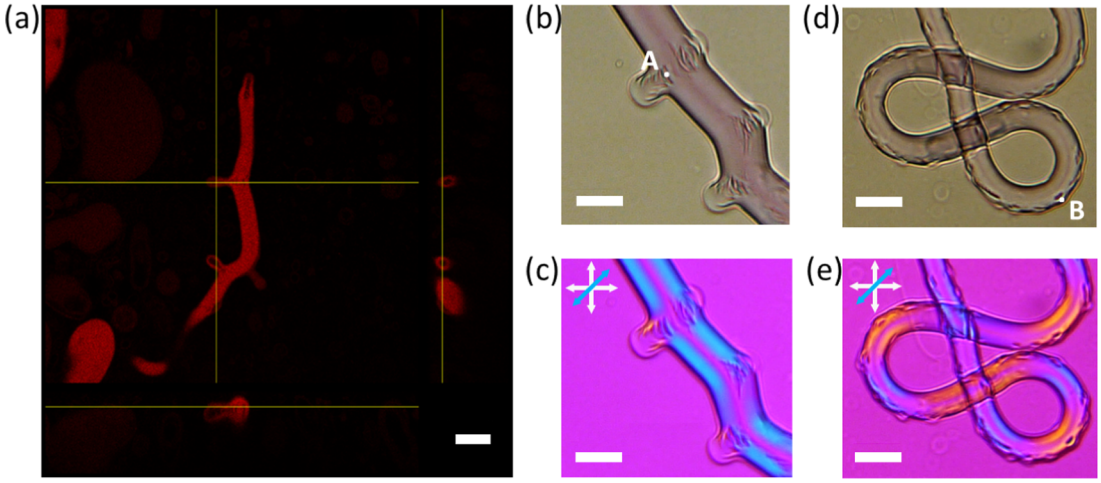

Figure 5. (a) Fluorescent image of myelin figures with side tubes. (b, d) Bright-field images and (c, e) the corresponding polarizing light microscopy images taken with a retardation plate at room temperature after heating to 60 °C at heating rates of (b, c) 1 °C/min and (d, e) 8 °C/min. The defects in the sample heated with lower and higher process rates are marked with "A" and "B", respectively. The arrows indicate the orientations of crossed polarizers (white double arrows) and the full-wavelength retardation plate's slow axis (blue double arrow). The scale bars are 10 μm.

view is noted in tubes growing from the lipid reservoir, while the explicit water core is present in tubes forming from the multilamellar regions. During the growth process, some tubes start to coil.[30] We observed that the looped structures are formed by the solid tubes, which are characterized by higher membrane tension compared to hollow tubes. These outcomes are pursuant to the theory of myelin coiling,[31] suggesting that multilamellar tubes characterized by substantial membrane tension are more prone to be twisted.

The orientational ordering of phospholipids was also verified by fluorescence confocal polarizing microscopy. In this work, DLPC was stained by NR molecules that self-align parallel to the hydrophobic tails of phospholipids. Therefore, by detecting the intensity of fluorescence emitted by NR for the given polarization direction of the incident laser beam, the orientation of DLPC could be determined. As illustrated in Figure 3a−c, the regions where the long axes of amphiphilic molecules are parallel to the laser beam polarization manifest themselves as the brightest part of the myelin tube. The lower-intensity regions correspond to lipid and dye molecules oriented with a certain deviation from the direction of the probing light's polarization, whereas the regions with molecules oriented orthogonally to the incident light were observed as the darkest part of the imaged cylindrical structure. Since Nile Red is a hydrophobic molecule, consequently, the water core running inside the myelin tube is clearly separated from the walls composed of stained lipid bilayers. It is important to note that these results are in good agreement with the findings obtained by polarized light microscope equipped with the retardation plate.

Several MFs took an oval form at the end of tube. In contrast to well-ordered lamellar rings obtained via the drying droplet experiment,[12,32] the myelin-like microstructures prepared by the contact experiment could be easily observed under a polarized light microscope (Figure 4b,c) due to a greater thickness of walls forming the tubes.

Subsequently, the sample was imaged by confocal fluorescence microscopy in two regions to investigate the morphology of myelin tubes ending exhibiting novel shapes. As illustrated in Figure 4d, the cross-sectional view (A) shows the collapsed MF in two directions. Besides, the structure contains the lipid free volume inside the rounded part of the lamellar phase, while its opposite walls are almost in contact with each other. This observation is consistent with the physical phenomena of collapse of thin- and thick-wall tubes.[12,33] Myelin-like instabilities are formed by regularly stacked bilayers that can slide with respect to each other; therefore, the shape of the tube may be modified. Flattening of the structure results in a reduction of the bending energy on the planar part, while higher bending energy cost is still localized on the edges of the oval part.[34] In contrast, Figure 4e,f shows a multilamellar structure, which is collapsed in one direction, giving the MF a spoonlike shape. The cross-sectional view (B) depicts that there is no visible core within this structure. It is noteworthy to mention that both MFs (Figure 4d,e) are formed from the solid tubes.

The following observations at room temperature showed the local disorder of lamellar orientation in some MFs. Holes are mainly noted in the bent regions of the lipid tubes. Importantly, this phenomenon occurs around 20 min after the step of the rapid growth of elongated lyotropic structures in systems stained by the fluorescent dye, while it needs more time to occur in the samples without the dye. Presumably, the organization of Nile Red molecules along lipid molecules affects the elastic properties of lamellar phase, facilitating such disrupted regions. A prior study has shown holes in lipid reservoir;[35] however, we observed a local disorder in some myelin tubes along their longitudinal axis. Surprisingly, the structural defects may lead to the formation of additional (hereafter called side) branched tubules. Both structures differ widely in their origins and dimensions, as shown in Figure 5a. First, main myelin tubes are formed at the dried lipid−water interface, whereas side myelin tubes grow spontaneously from the defects in stacked lipid bilayers. Besides, the primary myelin tubes grow faster than secondary myelin tubes, which are formed at least 20 min after water injection. This observation is in line with the previous report, which indicated that driving stress such as gradient of humidity has a significant impact on the rate of the growth.[11] Second, the ratio of diameter of side to primary elongated structure is about 0.6

https://dx.doi.org/10.1021/acs.jpcb.0c08907
J. Phys. Chem. B 2020, 124, 11974−11979

(average results out of 20 samples, measured within 1 h after cell preparation). Moreover, thinner tubules are characterized by the width-to-length ratio of about 0.4, while the aspect ratio for main myelin tubes is significantly lower.

Besides experiments at room temperature, we also investigated the influence of heating on the MFs. Hence, the liquid crystalline cell with MFs was heated to 90 °C without notable changes in lamellar phase (to preclude water boiling, higher temperatures were not examined). Further experiments were carried out up until 60 °C with distinct process rates. The first sample was heated at a rate of 1 °C/min, while the second sample was heated at a rate of 8 °C/min. As illustrated in Figure 5b,d, a large number of defects were noted in both samples after cooling to 20 °C. Interestingly, some short-side structures started to grow from the holes in multilamellar tubes of the first sample, whereas defects in the second sample remained unchanged. Besides, the surface along the edges of the second sample is densely covered with holes, while defect distribution of the first sample is more dispersed. In contrast to holes causing formation of side myelin tubes at room temperature, defects appearing after cooling down from high temperature can be predicted and limited in size to some extent. The combination of the heating and cooling processes affects the fluidity of the structure, indicating the tendency to defect formation. Hypothetically, local reorganization of phospholipid within the lamellar phase may be explained by differences in the compositional distribution at distinct temperatures.

CONCLUSIONS

We performed a detailed investigation of the various morphologies of lyotropic MFs. The combination of polarized light and confocal fluorescence microscopy allowed us to study the structural changes in lipid tubes. During the formation of lamellar mesophases composed of zwitterionic phospholipids stained by Nile Red in excess of water, lipid tubes showed different cross-sectional configurations due to the region from where they grew. These observations indicated that the explicit water core is observed only in myelin structures starting from the preformed multilamellar regions. As a result, we noted that looped structures growing directly from the lipid reservoir are formed by the tubes without the explicit internal water channel. Throughout this study, we also presented cross-sectional views of oval parts ending chosen lipid tubes. Additionally, we reported a spontaneous formation of side MFs from local disorder in the lamellar phase. Further examination showed that the presence of defects along the lipid tubes could be predicted by carrying out heat treatment. We anticipate that this work may contribute to the research on models of myelin in the biological system.

ASSOCIATED CONTENT

Supporting Information

The Supporting Information is available free of charge at https://pubs.acs.org/doi/10.1021/acs.jpcb.0c08907.

Time evolution of the length of myelin structure (Figure S1); width distributions of myelin structure (S2); and bright-field, polarized light, and fluorescence microscopy images (Figure S3) (PDF)

Z-projection of the fluorescent images of myelin figures ended with an oval shape with their cross-sectional views (MP4)

AUTHOR INFORMATION

Corresponding Author

Katarzyna Matczyszyn − *Advanced Materials Engineering and Modelling Group, Faculty of Chemistry, Wroclaw University of Science and Technology, 50-370 Wroclaw, Poland;* orcid.org/0000-0001-8578-8340; Phone: +48 71 320 40 08; Email: katarzyna.matczyszyn@pwr.edu.pl

Authors

Dominika Benkowska-Biernacka − *Advanced Materials Engineering and Modelling Group, Faculty of Chemistry, Wroclaw University of Science and Technology, 50-370 Wroclaw, Poland*

Ivan I. Smalyukh − *Department of Physics and Materials Science and Engineering Program, University of Colorado Boulder, Boulder, Colorado 80309, United States;* orcid.org/0000-0003-3444-1966

Complete contact information is available at: https://pubs.acs.org/10.1021/acs.jpcb.0c08907

Notes

The authors declare no competing financial interest.

ACKNOWLEDGMENTS

D.B.-B. thanks the BioTechNan program of interdisciplinary Ph.D. studies at Wroclaw University of Science and Technology for the support as well as the support from the Photonics and Bionanotechnology Association (PhoBiA). NCN Harmonia project DEC/2016/22/M/ST4/00275 and OPUS DEC/2019/35/B/ST4/03280 are also greatly acknowledged. Utilization of some of the described experiments from multimodal optical imaging facility at the University of Colorado Boulder was partially supported by the National Science Foundation grant DMR-1420736. The authors also thank H. Mundoor and B. Senyuk for discussion and technical assistance.

REFERENCES

(1) Dierking, I.; Neto, A. M. F. Novel Trends in Lyotropic Liquid Crystals. *Crystals* **2020**, *10*, 1−24.

(2) Lee, Y. S. Assembly of Lyotropic Liquid Crystals with Solid Crystal's Structural Order Translated from the Lipid Rafts in Cell Membranes. *J. Am. Chem. Soc.* **2017**, *139*, 17044−17051.

(3) Brach, K.; Hatakeyama, A.; Nogues, C.; Olesiak-Banska, J.; Buckle, M.; Matczyszyn, K. Photochemical Analysis of Structural Transitions in DNA Liquid Crystals Reveals Differences in Spatial Structure of DNA Molecules Organized in Liquid Crystalline Form. *Sci. Rep.* **2018**, *8*, No. 4528.

(4) Andersen, O. S.; Koeppe, R. E. Bilayer Thickness and Membrane Protein Function: An Energetic Perspective. *Annu. Rev. Biophys. Biomol. Struct.* **2007**, *36*, 107−130.

(5) Mitov, M. Cholesteric Liquid Crystals in Living Matter. *Soft Matter* **2017**, *13*, 4176−4209.

(6) Min, Y.; Kristiansen, K.; Boggs, J. M.; Husted, C.; Zasadzinski, J. A.; Israelachvili, J. Interaction Forces and Adhesion of Supported Myelin Lipid Bilayers Modulated by Myelin Basic Protein. *Proc. Natl. Acad. Sci. U.S.A.* **2009**, *106*, 3154−3159.

(7) Saher, G.; Brügger, B.; Lappe-Siefke, C.; Möbius, W.; Tozawa, R. I.; Wehr, M. C.; Wieland, F.; Ishibashi, S.; Nave, K. A. High Cholesterol Level Is Essential for Myelin Membrane Growth. *Nat. Neurosci.* **2005**, *8*, 468−475.

(8) Podbielska, M.; Banik, N. L.; Kurowska, E.; Hogan, E. L. Myelin Recovery in Multiple Sclerosis: The Challenge of Remyelination. *Brain Sci.* **2013**, *3*, 1282−1324.

(9) Boullerne, A. I. The History of Myelin. *Exp. Neurol.* **2016**, *283*, 431−445.
(10) Buchanan, M.; Egelhaaf, S. U.; Cates, M. E. Dynamics of Interface Instabilities in Nonionic Lamellar Phases. *Langmuir* **2000**, *16*, 3718−3726.
(11) Mosaviani, R.; Moradi, A. R.; Tayebi, L. Effect of Humidity on Liquid-Crystalline Myelin Figure Growth Using Digital Holographic Microscopy. *Mater. Lett.* **2016**, *173*, 162−166.
(12) Zou, L. N. Myelin Figures: The Buckling and Flow of Wet Soap. *Phys. Rev. E* **2009**, *79*, 1−10.
(13) Mishima, K.; Satoh, K.; Ogihara, T. The Effects of PH and Ions on Myelin Figure Formation in Phospholipid-Water System. *Chem. Phys. Lett.* **1984**, *106*, 513−516.
(14) Sakurai, I.; Kawamura, Y. Magnetic-Field-Induced Orientation and Bending of the Myelin Figures of Phosphatidylcholine. *Biochim. Biophys. Acta* **1983**, *735*, 189−192.
(15) Mishima, K.; Nakamae, S.; Ohshima, H.; Kondo, T. Frequency dependence of electric-field-induced orientation of myelin tubes. *Biochim. Biophys. Acta* **1994**, *1191*, 157−163.
(16) Tayebi, L.; Mozafari, M.; Vashaee, D.; Parikh, A. N. Structural Configuration of Myelin Figures Using Fluorescence Microscopy. *Int. J. Photoenergy* **2012**, *2012*, No. 4528.
(17) Kozlov, M. M.; Chernomordik, L. V. Membrane Tension and Membrane Fusion. *Curr. Opin. Struct. Biol.* **2015**, *33*, 61−67.
(18) Taribagil, R.; Arunagirinathan, M. A.; Manohar, C.; Bellare, J. R. Extended Time Range Modeling of Myelin Growth. *J. Colloid Interface Sci.* **2005**, *289*, 242−248.
(19) Jones, S.; Huynh, A.; Gao, Y.; Yu, Y. Calcium Ion-Assisted Lipid Tubule Formation. *Mater. Chem. Front.* **2018**, *2*, 603−608.
(20) Temgire, M. K.; Manohar, C.; Bellare, J.; Joshi, S. S. Structural Studies on Nonequilibrium Microstructures of Dioctyl Sodium Dodecyl Sulfosuccinate (Aerosol-OT) in p-Toluenesulfonic Acid and Phosphatidylcholine. *Adv. Phys. Chem.* **2012**, *2012*, 1−8.
(21) Huang, J. R.; Cheng, Y. C.; Huang, H. J.; Chiang, H. P. Confocal Mapping of Myelin Figures with Micro-Raman Spectroscopy. *Appl. Phys. A: Mater. Sci. Process.* **2018**, *124*, No. 58.
(22) Peddireddy, K.; Kumar, P.; Thutupalli, S.; Herminghaus, S.; Bahr, C. Myelin Structures Formed by Thermotropic Smectic Liquid Crystals. *Langmuir* **2013**, *29*, 15682−15688.
(23) Frolov, V. A.; Shnyrova, A. V.; Zimmerberg, J. Lipid Polymorphisms and Membrane Shape. *Cold Spring Harbor Perspect. Biol.* **2011**, *3*, No. a004747.
(24) Reissig, L.; Fairhurst, D. J.; Leng, J.; Cates, M. E.; Mount, A. R.; Egelhaaf, S. U. Three-Dimensional Structure and Growth of Myelins. *Langmuir* **2010**, *26*, 15192−15199.
(25) Kucherak, O. A.; Oncul, S.; Darwich, Z.; Yushchenko, D. A.; Arntz, Y.; Didier, P.; Mély, Y.; Klymchenko, A. S. Switchable Nile Red-Based Probe for Cholesterol and Lipid Order at the Outer Leaflet of Biomembranes. *J. Am. Chem. Soc.* **2010**, *132*, 4907−4916.
(26) Jana, B.; Ghosh, S.; Chattopadhyay, N. Competitive Binding of Nile Red between Lipids and β-Cyclodextrin. *J. Photochem. Photobiol., B* **2013**, *126*, 1−10.
(27) Smalyukh, I. I. Confocal Microscopy of Director Structures in Strongly Confined and Composite Systems. *Mol. Cryst. Liq. Cryst.* **2007**, *477*, 23/517−41/535.
(28) Sakurai, I.; Kawamura, Y. Growth Mechanism of Myelin Figures of Phosphatidylcholine. *Biochim. Biophys. Acta* **1984**, *777*, 347−351.
(29) Zhang, D.; Liu, Z.; Konetski, D.; Wang, C.; Worrell, B. T.; Bowman, C. N. Liposomes Formed from Photo-Cleavable Phospholipids: In Situ Formation and Photo-Induced Enhancement in Permeability. *RSC Adv.* **2018**, *8*, 14669−14675.
(30) Santangelo, C. D.; Pincus, P. Coiling Instabilities of Multilamellar Tubes. *Phys. Rev. E* **2002**, *66*, No. 061501.
(31) Huang, J. R. Theory of Myelin Coiling. *Eur. Phys. J. E* **2006**, *19*, 399−412.
(32) Zou, L. N.; Nagel, S. R. Stability and Growth of Single Myelin Figures. *Phys. Rev. Lett.* **2006**, *96*, No. 138301.
(33) Kozlovsky, P.; Zaretsky, U.; Jaffa, A. J.; Elad, D. General Tube Law for Collapsible Thin and Thick-Wall Tubes. *J. Biomech.* **2014**, *47*, 2378−2384.
(34) Lipowsky, R. The Conformation of Membranes. *Nature* **1991**, *349*, 475−481.
(35) Bhatia, T.; Hatwalne, Y.; Madhusudana, N. V. Tubular Growth and Bead Formation in the Lyotropic Lamellar Phase of a Lipid. *Soft Matter* **2015**, *11*, 5641−5646.

https://dx.doi.org/10.1021/acs.jpcb.0c08907
J. Phys. Chem. B 2020, 124, 11974−11979